Rapid Communications

Gapless spin liquid ground state of the spin-$\frac{1}{2}$ J_1-J_2 Heisenberg model on square lattices

Wen-Yuan Liu,[1,2] Shaojun Dong,[1,2] Chao Wang,[1,2] Yongjian Han,[1,2,*] Hong An,[3] Guang-Can Guo,[1,2] and Lixin He[1,2,†]

[1]*Key Laboratory of Quantum Information, University of Science and Technology of China, Hefei, Anhui 230026, China*

[2]*Synergetic Innovation Center of Quantum Information and Quantum Physics, University of Science and Technology of China, Hefei 230026, China*

[3]*School of Computer Science and Technology, University of Science and Technology of China, Hefei 230026, China*

(Received 18 June 2018; revised manuscript received 11 November 2018; published 17 December 2018)

The spin-$\frac{1}{2}$ J_1-J_2 Heisenberg model on square lattices is investigated via the finite projected entangled pair states (PEPS) method. Using the recently developed gradient optimization method combined with Monte Carlo sampling techniques, we are able to obtain the ground state energies that are competitive with the best results. The calculations show that there is no Néel order, dimer order, or plaquette order in the region of $0.42 \lesssim J_2/J_1 \lesssim 0.6$, suggesting a single spin liquid phase in the intermediate region. Furthermore, the calculated staggered spin, dimer, and plaquette correlation functions all have power law decay behaviors, which provide strong evidence that the intermediate nonmagnetic phase is a single gapless spin liquid state.

DOI: 10.1103/PhysRevB.98.241109

During the past decades, frustrated magnets have attracted enormous attention [1]. Frustrated interactions result in a large degeneracy of the ground state, and quantum fluctuations may lead to a massive coherent superposition of the degenerated states, implying a novel highly entangled (correlated) quantum state, known as a quantum spin liquid (QSL) [2–4], which lacks any long-range magnetic order even down to zero temperature. Because of the anomalously high degree of entanglement, QSLs have nontrivial topological properties which may host exotic excitations with fractional statistics, such as spinons, visions, etc., which have important applications in quantum computing [5,6].

The spin-$\frac{1}{2}$ J_1-J_2 Heisenberg model on square lattices is one of the primary candidate models to study the QSL, which was first introduced to describe the breakdown of Néel antiferromangetic (NAF) long-range order (LRO) in cuprate superconductors [7–9]. It is widely accepted that this model exhibits an NAF LRO at a small J_2/J_1 region and a collinear antiferromangetic LRO at large J_2/J_1, separated by a nonmagnetic phase in the region of $0.4 \lesssim J_2/J_1 \lesssim 0.6$.

Despite extensive investigations in the past three decades by various methods [8–33], the nature of the nonmagnetic region is still highly controversial. An early density matrix renormalization group (DMRG) study [24] suggested that the nonmagnetic region is a gapped Z_2 spin liquid phase. However, a more recent DMRG study with SU(2) symmetry [26] suggested a plaquette valence-bond (PVB) phase for $0.5 \lesssim J_2/J_1 \lesssim 0.61$ with a near critical region for $0.45 \lesssim J_2/J_1 \lesssim 0.5$. On the other hand, variational quantum Monte Carlo (vQMC) simulations [25] suggested the nonmagnetic region is a gapless QSL. Therefore, the understanding of the true nature of the nonmagnetic region is still far from complete.

The recently developed projected entangled pair states (PEPS) method [34] provides a powerful tool to simulate two-dimensional (2D) quantum many-body systems. Unlike the DMRG method, the PEPS satisfies area law in two dimensions, and therefore is a more natural way to study strongly correlated systems in two dimensions. However, PEPS methods suffer from an extremely high computational scaling to the virtual bond dimensions, and are very difficult to optimize.

Recently, we developed a finite PEPS optimization algorithm which combines the stochastic gradient optimization and Monte Carlo (MC) sampling techniques [35,36]. It can give a much higher precision than the simple update [37] and even full update methods [38], making it a reliable method to investigate the properties of the intermediate nonmagnetic phase.

In this Rapid Communication, we investigate the ground state of the nonmagnetic phases of the J_1-J_2 model using our recently developed finite PEPS methods. We find that for $0.42 \lesssim J_2/J_1 \lesssim 0.6$, the spin order, as well as the dimer order, all vanish in the thermodynamic limit, which rules out the possibility of valence-bond solid (VBS) states including PVB and a columnar valence bond (CVB) [33,39–41], and no additional phase transitions are found in this region. Furthermore, both the calculated spin-spin and dimer-dimer correlations show power law decays, suggesting that the region is a gapless QSL. These results are consistent with recent vQMC simulations [25].

The spin-$\frac{1}{2}$ J_1-J_2 Heisenberg model is given by

$$H = J_1 \sum_{\langle i,j \rangle} \mathbf{S}_i \cdot \mathbf{S}_j + J_2 \sum_{\langle\langle i,j \rangle\rangle} \mathbf{S}_i \cdot \mathbf{S}_j, \tag{1}$$

where $\langle i, j \rangle$ and $\langle\langle i, j \rangle\rangle$ denote the nearest-neighbor (NN) and the next-nearest-neighbor (NNN) spin pairs, respectively. We assume the exchange couplings $J_1, J_2 > 0$. Without loss of

*smhan@ustc.edu.cn
†helx@ustc.edu.cn

generality, we set $J_1 = 1$ throughout this Rapid Communication.

We study the system on an $L \times L$ square lattice with open boundary conditions, for L up to 16. We represent the ground state wave functions by PEPS with a virtual bond dimension D. All parameters in the PEPS wave functions are independent, and subject to optimization. When optimizing the PEPS, we first perform an imaginary time evolution with the simple update method [37]. We then further optimize the PEPS using the stochastic gradient method until the results are fully converged [35]. The energies and energy gradients are calculated via the MC sampling technique. The method greatly improves the ground state energies compared to the simple update and even full update method [38]. More details about the method can be found in Ref. [35]. With sufficiently optimized ground state PEPS wave functions, the physical quantities and correlation functions, including the staggered magnetization, dimer and plaquette order parameters, spin-spin correlations, dimer-dimer correlations, and plaquette-plaquette correlations, are calculated via Monte Carlo sampling techniques.

To guarantee the reliability of the calculations, the convergence to the virtual dimension D and the truncation dimension D_c during contractions is carefully checked. We find that $D = 8$, $D_c = 24$ are enough for systems up to 16×16 (see the Supplemental Material [42]). All results are obtained under these parameters, unless otherwise claimed.

The ground state energies at different J_2, particularly in the highly frustrated region, are important criteria for the precision of a computational method. We calculate ground state energies of different J_2 for system size $L = 4$–16. We then perform finite size scaling to obtain the ground state energies in the thermodynamic limit. In our previous studies [35], it has been shown for the Heisenberg model, i.e., $J_2 = 0$, the ground state energy per site obtained by $D = 10$ is $E_0 = -0.669\,48(42)$, in excellent agreement with the quantum Monte Carlo result $E_0 = -0.669\,437(5)$ [43]. We show the ground state energies for $J_2 = 0.5$ and 0.55 with different system sizes in Figs. 1(a) and 1(b), respectively. The extrapolated energies at the thermodynamic limit are $E_1 = -0.4966(1)$ for $J_2 = 0.5$ and $E_2 = -0.4861(1)$ for $J_2 = 0.55$. Some previously calculated ground state energies in the literature are also shown for comparison. The ground state energies obtained in this Rapid Communication are significantly lower than previous infinite PEPS (iPEPS) [31] results with $D = 7$ and the finite PEPS calculation with $D = 9$ and a periodic boundary condition (PBC) [30]. In the iPEPS calculations [31], a conjugated gradient optimization method was used but the wave functions are restricted to a single tensor with SU(2) symmetry. As for the finite PBC PEPS calculations [30], 2×2 unit cells were used and the ground states were obtained by the so-called cluster update. In our calculations, all tensors are independent and the ground states are obtained by the accurate gradient optimization method [35]. However, because different boundary conditions are used in these calculations, one cannot compare the energies directly, and therefore we only compare the energies extrapolated to the thermodynamic limit, which are listed in Table S3 of the Supplemental Material [42]. Our results with $D = 8$ can be treated as the upper bounds of the ground state energies, which are almost the same as the best DMRG results [26] $E_1 \simeq -0.4968$ and $E_2 \simeq -0.4863$, obtained by a rough estimation based on cylindrical geometries; they are also comparable to the energies from vQMC plus Lanczos extrapolation [25].

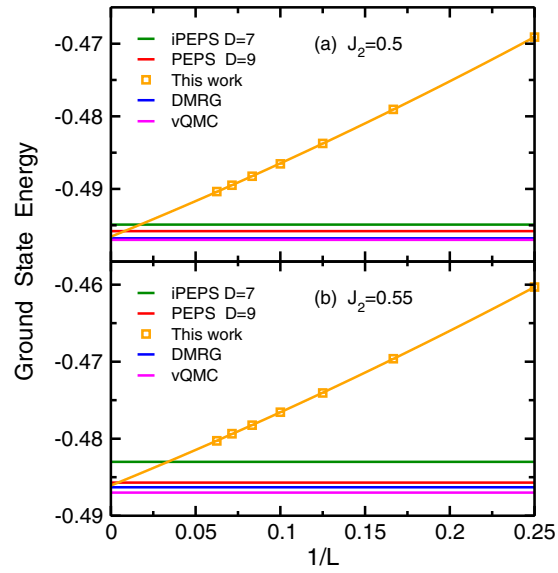

FIG. 1. Ground state energies in the 2D limit for (a) $J_2 = 0.5$ and (b) $J_2 = 0.55$ obtained by second-order polynomial extrapolations of the energies at $L = 4$–16. The horizontal straight lines denote the ground state energies from previous calculations in the literature, where the green, red, blue, and magenta lines are the ground state energies in the 2D limit obtained by iPEPS with $D = 7$ [31], finite PEPS $D = 9$ based on periodic systems [30], DMRG with SU(2) symmetry [26], and the variational quantum Monte Carlo plus Lanczos extrapolation [25]. The values of the ground state energies in the 2D limit are listed in Supplemental Material Table S3.

With the fully optimized ground states, we investigate the nature of the ground state. We first measure the Néel order parameter $m_s^2 = \frac{1}{N^2}\sum_{ij}\langle \mathbf{S}_i \cdot \mathbf{S}_j\rangle e^{i\mathbf{k}\cdot(\mathbf{r}_i-\mathbf{r}_j)}$ with $\mathbf{k} = (\pi, \pi)$ to distinguish the magnetic and the nonmagnetic phases at different J_2. To minimize the boundary effects, the summations are restricted in the central $W \times W$ lattice [35], and here $W = L - 4$ are used. At $J_2 = 0$, the calculated staggered magnetization is $m_{s,\infty} = 0.305$ [35], which is in excellent agreement with the QMC result $m_{s,\infty} = 0.307$ [43]. We present m_s^2 for different system sizes with $L = 8$–16 in Fig. 2, and m_s for the 2D limit in the inset of Fig. 2. These results suggest that the magnetic to nonmagnetic phase transition is located at $J_2 \simeq 0.42$, falling in the range of previous studies 0.41–0.45 [24–29].

However, the exact nature of the intermediate nonmagnetic phase is still hotly debated. We need to further clarify the nature of the nonmagnetic region, especially, to answer the following questions: Is the phase a QSL phase or a VBS phase? Is there a phase transition from QSL to VBS? We calculate the dimer structure factors which can be used to detect the possible VBS order,

$$M_d^{\alpha}(\mathbf{k}) = \frac{1}{N}\sum_{ijkl}\left(\left\langle B_{i,j}^{\alpha} B_{k,l}^{\alpha}\right\rangle - \left\langle B_{i,j}^{\alpha}\right\rangle\left\langle B_{k,l}^{\alpha}\right\rangle\right) e^{i\mathbf{k}\cdot(\mathbf{r}_i-\mathbf{r}_j)}, \quad (2)$$

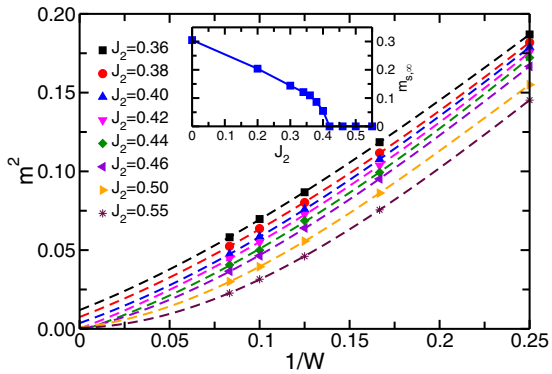

FIG. 2. The Néel order parameter m_s^2 calculated by PEPS with $D = 8$, on the $L = 8$, 10, 12, 14, and 16 square lattices where the central bulk size is $W = L - 4$. Extrapolations to the 2D limit are performed with a third-order polynomial fitting. The inset depicts the m_s in the thermodynamic limit at different J_2.

where $\alpha = x, y$, and $B^x_{i,j} = \mathbf{S}_{i,j} \cdot \mathbf{S}_{i+1,j}$ and $B^y_{i,j} = \mathbf{S}_{i,j} \cdot \mathbf{S}_{i,j+1}$ are horizontal and vertical bond operators along the x and y axis, respectively. The summation is restricted in the central bulk $W = L - 4$ to reduce the boundary effects. The VBS order is indicated by peaks appearing at $\mathbf{k} = (\pi, 0)$ for $M^x_d(\mathbf{k})$ or at $\mathbf{k} = (0, \pi)$ for $M^y_d(\mathbf{k})$. Therefore, one may define the horizontal and vertical dimer order parameters as $m^2_{dx} = \frac{1}{N} M^x_d(\mathbf{k})$ with $\mathbf{k} = (\pi, 0)$ and $m^2_{dy} = \frac{1}{N} M^y_d(\mathbf{k})$ with $\mathbf{k} = (0, \pi)$, respectively.

Figure 3 depicts the dimer order parameters m^2_{dx} and m^2_{dy}, calculated at two typical nonmagnetic points, $J_2 = 0.5$ and 0.55 with different system sizes. According to the deconfined quantum critical point (DQCP) theory [44], the complex order parameter $m_{dx} + i m_{dy}$ is sufficient to detect and distinguish both columnar and plaquette VBS phases. We find that m^2_{dx}

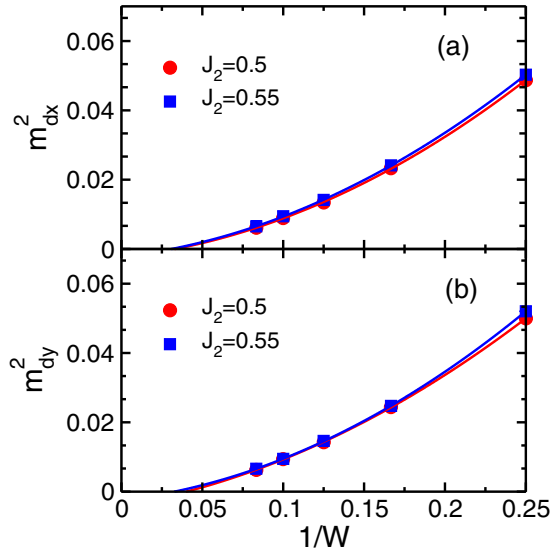

FIG. 3. The horizontal and vertical dimer order parameters (a) m^2_{dx} and (b) m^2_{dy} for $J_2 = 0.5$ and 0.55 with system sizes $L = 8$–16. Extrapolations are performed using second-order polynomial fittings.

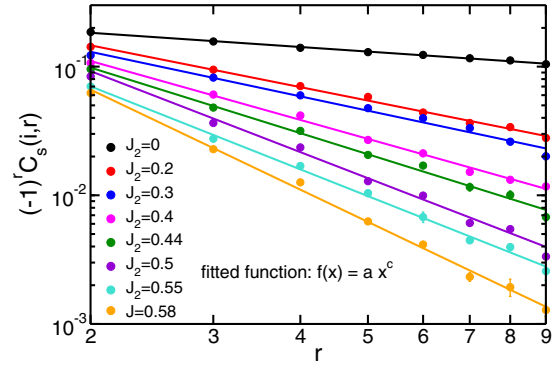

FIG. 4. Log-log plots of spin-spin correlation functions vs distance on a 14×14 lattice for different J_2.

and m^2_{dy} are almost the same within numerical precision at each lattice size, reflecting the isotropy of horizontal and vertical directions, which is expected for the true ground states and excludes the CVB phases. As a result, the disappearance of dimer orders in both the x and y directions does not support a VBS order at $J_2 = 0.5$ and 0.55 at the thermodynamic limit, which indicates that the whole intermediate nonmagnetic region is actually a QSL phase and there is no phase transition to the VBS phase, which is different from the results of Gong *et al.* [26]. Different choices of W such as $W = L - 4$, $L - 6$, and $L - 8$ lead to the same conclusions (see Supplemental Material [42]).

To further explore the properties of the QSL, more explicitly, whether it is gapped or gapless, we calculate the staggered spin-spin, dimer-dimer, and plaquette-plaquette correlation functions along straight lines.

The spin-spin correlation functions are calculated on a 14×14 lattice, and the results are averaged over the central $M = 6$ rows,

$$C_s(i, r) = \frac{1}{M} \sum_j \langle \mathbf{S}_{i,j} \cdot \mathbf{S}_{i+r,j} \rangle, \tag{3}$$

where j is restricted in the central M rows and i is fixed to 2. As shown in Fig. 4, the spin-spin correlations have a power law decay in a large parameter region, from $J_2 = 0$ to $J_2 = 0.58$. In the Néel phase, a long-range order will be exhibited, and spin correlations are expected to eventually decay to a saturation value theoretically. Due to our current computational limit, we cannot access larger systems to observe such a saturation value, but it is notable that at $J_2 = 0$ the absolute value of $C_s(i, r = 9) \simeq 0.102$ on a 14×14 lattice is very close to the QMC value $C_s(i, r \to \infty) \simeq 0.094$ on an infinite system [43], indicating the calculated power law decay behavior of spin-spin correlations obtained from finite systems for the Néel phase ($J_2 \lesssim 0.42$) is reliable to some extent. The power law decay behaviors in the QSL phase imply that there is no $\mathbf{S} = 1$ gap in the 2D limit. The spin-spin correlation behaviors are consistent with the lack of VBS orders in the intermediate phase, in which the $\mathbf{S} = 1$ gap is expected. The power law decay exponents for different J_2 are listed in Table S4 of the Supplemental Material [42], which increase with increasing J_2. We note that the decay exponents

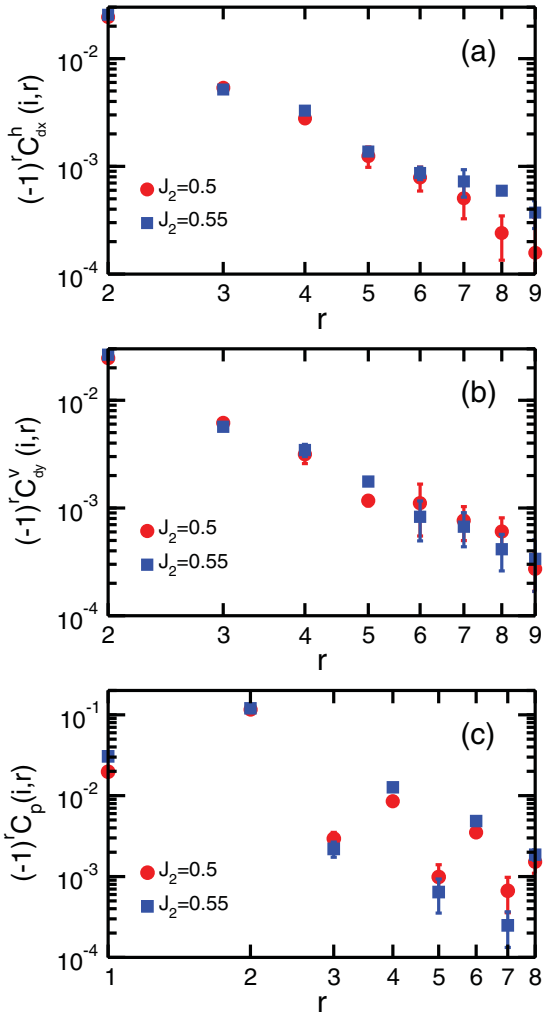

FIG. 5. Log-log plots of (a) the horizontal dimer-dimer correlation functions along the x axis, (b) the vertical dimer-dimer correlation functions along the y axis, and (c) the plaquette-plaquette correlation functions along the x axis on a 16×16 lattice at $J_2 = 0.5$ and 0.55.

fitted from the finite systems here should not be compared directly to those of the infinite systems.

We further calculate the dimer-dimer and plaquette-plaquette correlation functions. The horizontal dimer-dimer correlations are defined as

$$C^h_{dx}(i,r) = \frac{1}{M}\sum_j \left(\left\langle B^x_{i,j} B^x_{i+r,j}\right\rangle - \left\langle B^x_{i,j}\right\rangle\left\langle B^x_{i+r,j}\right\rangle\right). \quad (4)$$

Similarly, we can define the vertical dimer-dimer correlations. The plaquette-plaquette correlations are defined as

$$C_p(i,r) = \frac{1}{M}\sum_j (\langle Q_{i,j} Q_{i+r,j}\rangle - \langle Q_{i,j}\rangle\langle Q_{i+r,j}\rangle), \quad (5)$$

where $Q_{i,j} = \frac{1}{2}(P_{\square,i,j} + P^{-1}_{\square,i,j})$ and $P_{\square,i,j}$ denotes the cyclic exchange operator of the four spins on a given plaquette. All correlation functions are averaged in the central $M = 4$ odd rows on 16×16 squares lattice and $i = 3$.

Figures 5(a)–5(c) depict the staggered horizontal, vertical dimer-dimer correlations, and plaquette-plaquette correlations, respectively, at two typical points $J_2 = 0.5$ and 0.55. We find that both the dimer-dimer and plaquette-plaquette correlation functions have a power law decay, indicating that there is no spin $\mathbf{S} = 0$ gap. The fitted power law decay exponents are about 2.8 for the dimer correlations. The plaquette correlation functions show large oscillations for odd and even r, which might have a close relation with the local plaquette order existing in the finite system. The fitted power law decay exponents are about 1.8–2.0 if only odd sites are used, and about 3.0 if only even sites are used in the fit.

The above results give strong evidence that the intermediate nonmagnetic phase is a gapless QSL, because there are no columnar orders or plaquette orders, and all correlation functions including spin-spin, dimer-dimer, and plaquette-plaquette correlations have power law decays. These results are consistent with the conclusions of recent vQMC simulations [25], which directly calculate the spin gaps. Recent DMRG calculations also suggest that there is a gapless spin liquid region [32] in $0.45 \lesssim J_2 \lesssim 0.52$. The major difference is that DMRG calculations suggest that there is another VBS state between $0.5 \lesssim J_2 \lesssim 0.61$ [26] with a spin $\mathbf{S} = 1$ gap, which is absent in our calculations. One of the possible reasons for the difference between the two works is that in the DMRG calculations, cylindrical boundary conditions are used, and also because of the quasi-one-dimensional (1D) nature of the DMRG method, the C_{4v} symmetry of the system is explicitly broken, which may favor some ordered states. We note that a recent iPEPS study with U(1) symmetry shows that the intermediate phase is a CVB [33], while our results based on finite square lattices show the horizontal and vertical directions are isotropic and there is no CVB order.

To summarize, we investigate the phase diagram of a spin-$\frac{1}{2}$ J_1-J_2 model on a square lattice using finite PEPS methods. The recent developed stochastic gradient method allows us to obtain highly accurate ground state energies and wave functions. The absence of spin and dimer orders together with a power law decay of the correlation functions present strong evidence that the intermediate nonmagnetic phase is a gapless spin liquid. Indeed, recently there has been some experimental evidence supporting such a gapless QSL state on the square lattice [45]. However, since the correlation functions have large correlation lengths in the nonmagnetic region, we cannot totally exclude the possibility of the existence of a very weak VBS order in the nonmagnetic phase, which may need significantly larger system sizes that go beyond our current capability. We hope further developed tensor network methods can access larger systems to reexamine these different scenarios.

We would like to thank L. Wang and S.-S. Gong for helpful discussions, and particularly thank Z.-C. Gu for extensive discussions. L.H. was supported by the National Key Research and Development Program of China (Grant No. 2016YFB0201202), and Y.H. was supported by the National Science Foundation of China (Grant No. 11474267). The numerical calculations have been done at the USTC HPC facilities.

[1] *Introduction to Frustrated Magnetism: Materials, Experiments, Theory*, edited by C. Lacroix, P. Mendels, and F. Mila (Springer, Berlin, 2011).
[2] P. Anderson, Mater. Res. Bull. **8**, 153 (1973).
[3] P. W. Anderson, Science **235**, 1196 (1987).
[4] L. Balents, Nature (London) **464**, 199 (2010).
[5] A. Kitaev, Ann. Phys. **303**, 2 (2003).
[6] A. Kitaev, Ann. Phys. **321**, 2 (2006).
[7] M. Inui, S. Doniach, and M. Gabay, Phys. Rev. B **38**, 6631 (1988).
[8] P. Chandra and B. Doucot, Phys. Rev. B **38**, 9335 (1988).
[9] E. Dagotto and A. Moreo, Phys. Rev. Lett. **63**, 2148 (1989).
[10] F. Figueirido, A. Karlhede, S. Kivelson, S. Sondhi, M. Rocek, and D. S. Rokhsar, Phys. Rev. B **41**, 4619 (1990).
[11] H. J. Schulz and T. A. L. Ziman, Europhys. Lett. **18**, 355 (1992).
[12] T. Einarsson and H. J. Schulz, Phys. Rev. B **51**, 6151 (1995).
[13] H. J. Schulz, T. A. L. Ziman, and D. Poilblanc, J. de Phys. I **6**, 675 (1996).
[14] N. E. Ivanov and P. C. Ivanov, Phys. Rev. B **46**, 8206 (1992).
[15] J. Sirker, Z. Weihong, O. P. Sushkov, and J. Oitmaa, Phys. Rev. B **73**, 184420 (2006).
[16] K. S. D. Beach, Phys. Rev. B **79**, 224431 (2009).
[17] V. Murg, F. Verstraete, and J. I. Cirac, Phys. Rev. B **79**, 195119 (2009).
[18] M. Mambrini, A. Läuchli, D. Poilblanc, and F. Mila, Phys. Rev. B **74**, 144422 (2006).
[19] L. Capriotti and S. Sorella, Phys. Rev. Lett. **84**, 3173 (2000).
[20] L. Capriotti, F. Becca, A. Parola, and S. Sorella, Phys. Rev. Lett. **87**, 097201 (2001).
[21] D. Schmalfuss, R. Darradi, J. Richter, J. Schulenburg, and D. Ihle, Phys. Rev. Lett. **97**, 157201 (2006).
[22] F. Mezzacapo, Phys. Rev. B **86**, 045115 (2012).
[23] R. Darradi, O. Derzhko, R. Zinke, J. Schulenburg, S. E. Krüger, and J. Richter, Phys. Rev. B **78**, 214415 (2008).
[24] H.-C. Jiang, H. Yao, and L. Balents, Phys. Rev. B **86**, 024424 (2012).
[25] W.-J. Hu, F. Becca, A. Parola, and S. Sorella, Phys. Rev. B **88**, 060402 (2013).
[26] S.-S. Gong, W. Zhu, D. N. Sheng, O. I. Motrunich, and M. P. A. Fisher, Phys. Rev. Lett. **113**, 027201 (2014).
[27] C.-P. Chou and H.-Y. Chen, Phys. Rev. B **90**, 041106 (2014).
[28] S. Morita, R. Kaneko, and M. Imada, J. Phys. Soc. Jpn. **84**, 024720 (2015).
[29] J. Richter, R. Zinke, and D. J. J. Farnell, Eur. Phys. J. B **88**, 2 (2015).
[30] L. Wang, Z.-C. Gu, F. Verstraete, and X.-G. Wen, Phys. Rev. B **94**, 075143 (2016).
[31] D. Poilblanc and M. Mambrini, Phys. Rev. B **96**, 014414 (2017).
[32] L. Wang and A. W. Sandvik, Phys. Rev. Lett. **121**, 107202 (2018).
[33] R. Haghshenas and D. N. Sheng, Phys. Rev. B **97**, 174408 (2018).
[34] F. Verstraete and J. I. Cirac, arXiv:cond-mat/0407066.
[35] W.-Y. Liu, S.-J. Dong, Y.-J. Han, G.-C. Guo, and L. He, Phys. Rev. B **95**, 195154 (2017).
[36] L. He, H. An, C. Yang, F. Wang, J. Chen, C. Wang, W. Liang, S. Dong, Q. Sun, W. Han, W. Liu, Y. Han, and W. Yao, IEEE Transactions on Parallel and Distributed Systems **29**, 2838 (2018).
[37] H. C. Jiang, Z. Y. Weng, and T. Xiang, Phys. Rev. Lett. **101**, 090603 (2008).
[38] M. Lubasch, J. I. Cirac, and M.-C. Bañuls, Phys. Rev. B **90**, 064425 (2014).
[39] S. Sachdev and R. N. Bhatt, Phys. Rev. B **41**, 9323 (1990).
[40] A. V. Chubukov and T. Jolicoeur, Phys. Rev. B **44**, 12050 (1991).
[41] R. R. P. Singh, Z. Weihong, C. J. Hamer, and J. Oitmaa, Phys. Rev. B **60**, 7278 (1999).
[42] See Supplemental Material at http://link.aps.org/supplemental/10.1103/PhysRevB.98.241109 for more details of the calculations, which includes Refs. [18,25,26,30,31,35,38,46,47].
[43] A. W. Sandvik, Phys. Rev. B **56**, 11678 (1997).
[44] T. Senthil, A. Vishwanath, L. Balents, S. Sachdev, and M. P. A. Fisher, Science **303**, 1490 (2004).
[45] O. Mustonen, S. Vasala, E. Sadrollahi, K. P. Schmidt, C. Baines, H. C. Walker, I. Terasaki, F. J. Litterst, E. Baggio-Saitovitch, and M. Karppinen, Nat. Commun. **9**, 1085 (2018).
[46] F. Verstraete, V. Murg, and J. Cirac, Adv. Phys. **57**, 143 (2008).
[47] A. W. Sandvik, Phys. Rev. B **85**, 134407 (2012).